VSP

*Advanced Composite Materials 18 (2009) 105–119*

ADVANCED COMPOSITE MATERIALS
www.brill.nl/acm

# Theory of Thin-Walled, Pretwisted Composite Beams with Elastic Couplings

**Sung Nam Jung** [a,*], **Chang-Joo Kim** [a], **Jin Hwan Ko** [a] **and Chang-Wan Kim** [b]

[a] Department of Aerospace Information Engineering, Konkuk University, Seoul 143-701, Republic of Korea

[b] Department of Mechanical Engineering, Konkuk University, Seoul 143-701, Republic of Korea

Received 11 January 2008; accepted 2 April 2008

**Abstract**

In this work, the structural response of thin-walled composite beams with pretwist angle is investigated by using a mixed beam approach that combines the stiffness and flexibility methods in a unified manner. The Reissner's semi-complimentary energy functional is used to derive the stiffness matrix that approximates the beam in an Euler–Bernoulli level for extension and bending and Vlasov level for torsion. The bending and torsion-related warpings induced by the pretwist effects are derived in a closed form. The developed theory is validated with available literature and detailed finite element structural analysis results using the MSC/NASTRAN. Pretwisted composite beams with rectangular solid and thin-walled box sections are illustrated to validate the current approach. Acceptable correlation has been achieved for cases considered in this study. The effects of pretwist and fiber orientation angles on the static behavior of pretwisted composite beams are also studied.



**Keywords**

Thin-walled blade, pretwist angle, mixed beam approach, warpings

## 1. Introduction

During the past couple of decades, pretwisted blades have attracted a lot of attention especially for helicopters, propellers, tilt rotors, and wind turbine applications. In a structural point of view, the pretwist affects not only on the torsional property but also on the bending rigidity. Besides the direct effect, the pretwist introduces a coupling between extension and torsion from a geometric origin, even for blades with isotropic materials. For the composite materials case, there will be an additional coupling between bending and torsion, or between extension and torsion, depending upon the layup geometry used in the structure. It is apparent that these

* To whom correspondence should be addressed. E-mail: snjung@konkuk.ac.kr
Edited by KPCM

 DOI:10.1163/156855109X428736

structural couplings make the analysis more involved than that without the pretwist effect, especially with composite materials.

Rosen [1] presented an extensive review covering statics, dynamics, and stability aspects of pretwisted beams. It is suggested that the appropriate treatment of sectional warpings (e.g., torsion warping) is viable for refined structural analysis of pretwisted blades. In addition to the torsion warpings, bending-related warpings can play significant roles in the structural response of thin-walled composite blades; thus, these warpings should be taken into account whenever they are relevant. Despite the considerable research activities undertaken so far [2–4], as pointed out by Yu [5], there remains still a lack of published results with which to compare for pretwisted composite beams. In other words, there is a strong need to provide benchmark results in the relevant fields and also fundamental information on specific subjects inherent in the modeling of pretwisted composite beams.

In the present work, a mixed-based approach is adopted for the structural response of thin-walled composite beams with built-in twist. The analytical model includes the effects of elastic couplings, shell wall thickness, torsion warping, and warping restraints. The bending and torsion-related warpings induced by the pretwist angles are derived in a closed form in the beam formulation. An extensive validation study is carried out to correlate the current analysis with available literature and also with detailed finite element structural analysis results. The effects of pretwist and fiber orientation angles on the static behavior of thin-walled composite beams are addressed in this study.

## 2. Formulation

Figure 1 shows the geometry and coordinate systems of a pretwisted beam. The pretwist effect is represented by a rotation $\beta(x)$ which is assumed as uniform ($\mathrm{d}\beta/\mathrm{d}x = k_1$) along the beam span. The pretwist angle at any spanwise location $x$ is given by:

$$\beta(x) = \beta_{\mathrm{T}} \cdot x/l, \tag{1}$$

where $\beta_{\mathrm{T}}$ is pretwist angle at the tip and $l$ is the length of a beam. Several sets of coordinate axes are employed to describe the motion. The first system is the $(x, y, z)$ system used to define the reference beam axis. The second system is the $(x, \eta, \varsigma)$ system where $(\eta, \varsigma)$ are the principal axes of the beam cross-section. The two coordinate axes are of the relation:

$$\begin{Bmatrix} x \\ y \\ z \end{Bmatrix} = \begin{bmatrix} 1 & 0 & 0 \\ 0 & \cos\beta & -\sin\beta \\ 0 & \sin\beta & \cos\beta \end{bmatrix} \begin{Bmatrix} x \\ \eta \\ \zeta \end{Bmatrix}. \tag{2}$$

Finally, a curvilinear coordinate system $(x, s, n)$ is defined for the section, where $s$ is the contour coordinate measured along the middle surface of the shell wall and $n$ is normal to the contour coordinate. The global deformations of the beam are $(U, V, W)$ along the $x$, $y$ and $z$ axes, respectively, and $\phi$ is the elastic twist. The

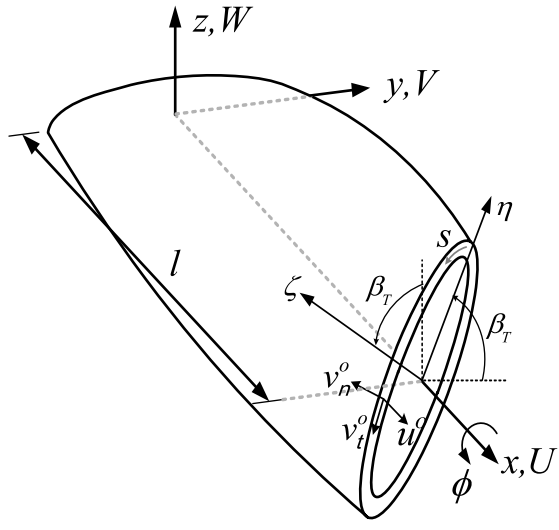


**Figure 1.** Geometry and coordinate systems of a pretwisted blade.

local shell deformations are $(u, v_t, v_n)$ along the $x, s$ and $n$ axes, respectively, and they are expressed as:

$$\begin{aligned} u &= u^0 + n\psi_x, \\ v_t &= v_t^0 + n\psi_s, \\ v_n &= v_n^0, \end{aligned} \tag{3}$$

where the superscript 0 denotes values defined at the mid-plane of the shell wall and $\psi_x, \psi_s$ represent rotations about the $s$- and $x$-axes, respectively. The shell mid-plane displacements are obtained *via* beam displacements and rotations from a geometric consideration (see Fig. 1):

$$\begin{aligned} v_t^0 &= Vy_{,s} + Wz_{,s} + r\phi, \\ v_n^0 &= Vz_{,s} - Wy_{,s} - q\phi, \\ \psi_s &= \phi, \end{aligned} \tag{4}$$

where $r$ and $q$ are the coordinates of an arbitrary point on the shell wall in the $(n, s)$ coordinate system, respectively, and the comma denotes the differentiation with respect to the coordinate. The strain–displacement and curvature–displacement relations for the thin shell segment are given by [6]:

$$\begin{Bmatrix} \varepsilon_{xx} \\ \varepsilon_{ss} \\ \gamma_{xs} \end{Bmatrix} = \begin{Bmatrix} u^0_{,x} \\ v^0_{t,s} \\ u^0_{,s} + v^0_{t,x} \end{Bmatrix}, \tag{5}$$

$$\begin{Bmatrix} \kappa_{xx} \\ \kappa_{ss} \\ \kappa_{xs} \end{Bmatrix} = \begin{Bmatrix} -v^0_{n,xx} \\ -v^0_{n,ss} \\ -2v^0_{n,xs} \end{Bmatrix}. \tag{6}$$

The membrane shear strain $\gamma_{xs}$ can be written from the beam kinematic relation and also from (4) and (5),

$$\gamma_{xs} = \eta_{,s}\gamma_{x\eta} + \zeta_{,s}\gamma_{x\zeta} = u^0_{,s} + \eta_{,s}V_{,x} + \zeta_{,s}W_{,x} + r\phi_{,x}. \tag{7}$$

Assuming the hoop stress flow $N_{ss}$ in the shell wall of the section is negligibly small and introducing a semi-inverted form of constitutive relations, one can obtain the following equations [7]:

$$\begin{Bmatrix} N_{xx} \\ M_{xx} \\ M_{xs} \\ \gamma_{xs} \\ \kappa_{ss} \end{Bmatrix} = \begin{bmatrix} C_{n\varepsilon} & C_{n\kappa} & C_{n\phi} & C_{n\gamma} & C_{n\tau} \\ C_{n\kappa} & C_{m\kappa} & C_{m\phi} & C_{m\gamma} & C_{m\tau} \\ C_{n\phi} & C_{m\phi} & C_{\phi\phi} & C_{\phi\gamma} & C_{\phi\tau} \\ -C_{n\gamma} & -C_{m\gamma} & -C_{\phi\gamma} & C_{\gamma\gamma} & C_{\gamma\tau} \\ -C_{n\tau} & -C_{m\tau} & -C_{\phi\tau} & C_{\gamma\tau} & C_{\tau\tau} \end{bmatrix} \begin{Bmatrix} \varepsilon_{xx} \\ \kappa_{xx} \\ \kappa_{xs} \\ N_{xs} \\ M_{ss} \end{Bmatrix}, \tag{8}$$

where the coefficients $C_{ij}$ can be found in Jung *et al.* [8]. As is expressed in (8), the shear flow and hoop moment resultants $N_{xs}$, $M_{ss}$ are treated as unknowns along with the shell strain measures: $\varepsilon_{xx}, \kappa_{xx}, \kappa_{xs}$. These $N_{xs}$, $M_{ss}$ will be determined by considering the equilibrium equations of the shell wall.

By equating the membrane shear strain $\gamma_{xs}$ defined respectively in (7) and (8) and integrating from 0 to $s$, one obtains the first approximation to the axial deformation $u^0$ as:

$$u^0 = U + (\eta\cos\beta - \zeta\sin\beta)\beta_y + (\eta\sin\beta + \zeta\cos\beta)\beta_z + \lfloor\psi_i\rfloor\{q\}, \tag{9}$$

where $\beta_y, \beta_z$ are the cross-section rotations, $\psi_i$ denote the cross-section warping functions subjected to constraint conditions for a closed thin-walled section as: $\oint \psi_i \,\mathrm{d}s = 0$. The generalized beam deformation vector $\{q\}$ appeared in (8) is defined as:

$$\{q\} = \lfloor U_{,x} \quad \beta_{y,x} \quad \beta_{z,x} \quad \phi_{,x} \quad \phi_{,xx} \rfloor^{\mathrm{T}}. \tag{10}$$

By substituting (9) into (4) and (5), the strain–displacement relations are expressed as a function of the beam displacement derivatives as:

$$\begin{aligned} \varepsilon_{xx} &= U_{,x} + (\eta\sin\beta + \zeta\cos\beta)\beta_{y,x} + (-\eta\cos\beta + \zeta\sin\beta)\beta_{z,x} \\ &\quad + \lfloor k_1(\eta\psi_{i,\zeta} - \zeta\psi_{i,\eta})\rfloor\{q\}, \\ \kappa_{xx} &= -(\zeta_{,s}\cos\beta + \eta_{,s}\sin\beta)\beta_{z,x} + (\zeta_{,s}\sin\beta - \eta_{,s}\cos\beta)\beta_{y,x} + q\phi_{,xx}, \\ \kappa_{xs} &= 2\phi_{,x}, \end{aligned} \tag{11}$$

where $\varepsilon_{xx}, \kappa_{xx}, \kappa_{xs}$ are the membrane and thickness shell strain measures, respectively, and $k_1$ is the rate of pretwist.

The stiffness matrix relating beam forces to beam displacements can be obtained by using a variational statement given by,

$$\delta\int_0^l \oint \{\Phi_R + \gamma_{xs}N_{xs} + \kappa_{ss}M_{ss}\}\,\mathrm{d}s\,\mathrm{d}x = 0, \tag{12}$$

where $l$ is the length of the blade and $\Phi_R$ is a modified form of the Reissner functional which is defined as:

$$\begin{aligned}\Phi_R = \frac{1}{2}\big(&A_{n\varepsilon}\varepsilon_{xx}^2 + 2A_{n\kappa}\kappa_{xx}\varepsilon_{xx} + 2A_{n\phi}\kappa_{xs}\varepsilon_{xx} + 2A_{n\gamma}N_{xs}\varepsilon_{xx} + 2A_{n\tau}M_{ss}\varepsilon_{xx}\\ &+ A_{m\kappa}\kappa_{xx}^2 + 2A_{m\phi}\kappa_{xx}\kappa_{xs} + 2A_{m\gamma}\kappa_{xx}N_{xs} + 2A_{m\tau}\kappa_{xx}M_{ss} + A_{\phi\phi}\kappa_{xs}^2\\ &+ 2A_{\phi\gamma}\kappa_{xs}N_{xs} + 2A_{\phi\tau}\kappa_{xs}M_{ss} + A_{xn}\gamma_{xn}^2 - A_{\gamma\gamma}N_{xs}^2\\ &- 2A_{\gamma\tau}N_{xs}M_{ss} - A_{\tau\tau}M_{ss}^2\big).\end{aligned} \tag{13}$$

Integrating (12) by parts with $x$ and using (4) and (5) result in the equilibrium equations for an element of the shell wall,

$$\begin{aligned}&N_{xx,x} + N_{xs,s} = 0,\\ &N_{xs,x} = 0,\\ &M_{xx,x} + M_{xs,s} = 0,\\ &M_{xs,x} + M_{ss,s} = 0.\end{aligned} \tag{14}$$

The first two equations in (14) indicate that $N_{xs}$ consists of a constant part and a part that depends on the $s$-integral of $N_{xx,x}$. Also, it is found from the third and fourth equations that $M_{ss}$ has a constant part, a part that varies linearly with $s$ and a part that depends on the $s$-integral of $M_{xs,x}$. Hence, one can write:

$$\begin{aligned}N_{xs} &= N_{xs}^0 - \int_0^s N_{xx,x}\,\mathrm{d}s,\\ M_{ss} &= M_{ss}^0 + yM_{ss}^y + zM_{ss}^z - \int_0^s M_{xs,x}\,\mathrm{d}s,\end{aligned} \tag{15}$$

where $N_{xs}^0$, $M_{ss}^0$, $M_{ss}^y$, $M_{ss}^z$ represent the circuit shear flows and hoop moments that need to be determined. Let us write the shear flows and hoop moments in a vector form as:

$$\{n\} = \lfloor\, N_{xs}^0 \quad M_{ss}^0 \quad M_{ss}^y \quad M_{ss}^z \,\rfloor^{\mathrm{T}}. \tag{16}$$

The continuity condition that must be satisfied for a closed profile yields the following four equations:

$$\oint \gamma_{xs}\,\mathrm{d}s = 2A_0\phi_{,x}, \qquad \oint \kappa_{ss}\,\mathrm{d}s = 0, \qquad \oint y\kappa_{ss}\,\mathrm{d}s = 0, \qquad \oint z\kappa_{ss}\,\mathrm{d}s = 0, \tag{17}$$

where $A_0$ is the enclosed area of the section. It is noted that, for a $m$-celled section, the continuity conditions lead to a set of $4m$ equations. Jung *et al.* [8] made an assessment for uniform beams with multiple-celled sections. For a two-cell section, a total of 8 continuity equations can be obtained. Substituting (8) into (17), the circuit shear flows and hoop moments are obtained as

$$\{n\} = [Q]^{-1}[P]\{q\} = [e]\{q\}, \tag{18}$$

where $[Q]$ is a symmetric $[4 \times 4]$ matrix and $[P]$ is a fully populated $[4 \times 5]$ matrix. By substituting (18) into (12), the unknown shear flows and hoop moments $N_{xs}$ and $M_{ss}$ are obtained as:

$$\left\{ \begin{array}{c} N_{xs} \\ M_{ss} \end{array} \right\} = [f]\{q\}. \tag{19}$$

The $[f]$ that appears in (19) corresponds to the active components of shear flows according to the terminology adopted in Gjelsvik [9]. So far, the unknown shear flow and hoop moment resultants are derived as a function of beam displacement derivatives. These relations are used to construct the beam force–displacement relations as in the classical stiffness-based approach. This is done by inserting (8) and (19) into (12) whereupon the final equations are written in a form:

$$\{F\} = [K]\{q\}, \tag{20}$$

where $[K]$ is the cross-sectional stiffness matrix and $\{F\}$ is the generalized beam force vector given by the relation,

$$\{F\} = \lfloor N \quad M_y \quad M_z \quad T \quad M_\omega \rfloor^{\mathrm{T}}, \tag{21}$$

where $N$ is the axial force, $M_y$ and $M_z$ are the bending moments about the $y$ and $z$ directions, respectively, $T$ is the twisting moment and $M_\omega$ is the Vlasov bi-moment. The $[5 \times 5]$ matrix that appears in (20) approximates the cross-section stiffness matrix $[K]$ at an Euler–Bernoulli level for extension and bending and a Vlasov level for torsion and include the influence of the shell wall thickness.

## 3. Results and Discussion

Prior to the main discussion, there is a need to check whether the warping functions appeared in (9) satisfy the constraint conditions given by the relation: $\oint \psi_i \, \mathrm{d}s = 0$. It is noted that the integration runs along the mid-line contour of a section wall. A single-cell thin-walled box section is chosen as an example. Each wall of the box section consists of $[15_6]$ layup. For convenience, the integration starts at the midpoint in the right wall where the symmetry axis is located (see Fig. 2). It is noted that, at this specific location, the section warpings should be zero. In Fig. 3, results showing the distribution of respective warping functions are presented with the contour coordinate. It is observed that, as the integration continues and reaches its original location, all the section integrals become identically zero. Thus the constraint conditions of the warping functions become satisfied and, further, the warping functions associated with the pretwist effects are taken into account appropriately in the beam formulation. In the remaining parts of this section, the efficacy of the proposed beam theory and also the influence of pretwist and fiber angles on the static behavior of composite beams will be discussed.

The first example considered is a pretwisted steel beam that used in the work of Durocher and Kane [10]. The length of the beam is 76.2 mm and has a rectangular solid section with a width of 25.4 mm and a thickness of 2.54 mm. The material

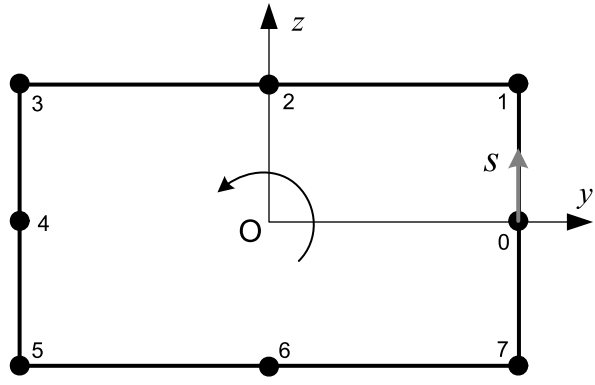


**Figure 2.** Control points of a single-cell box section.

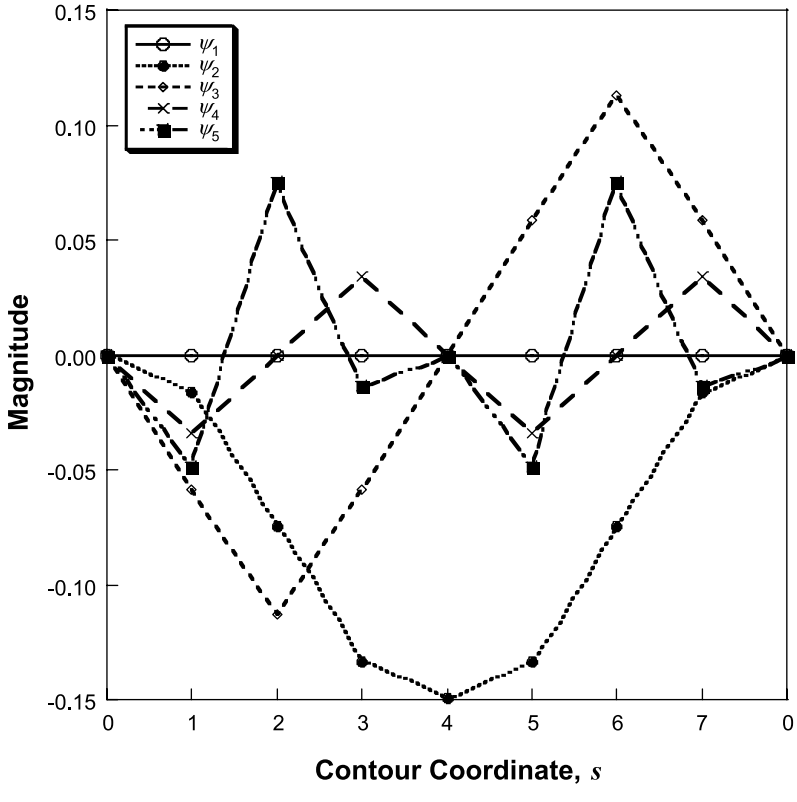


**Figure 3.** Variation of contour warping functions for thin-walled box section.

properties are: Young's modulus $E = 203.4$ MPa and Poisson's ratio $\nu = 0.3532$. The total geometric pretwist angle $\beta_T$ from root to tip of the beam is 68.8°. The beam is clamped at its root and is loaded at the beam tip. Figure 4 presents the comparison results of both the axial displacements and induced tip twist deformation for

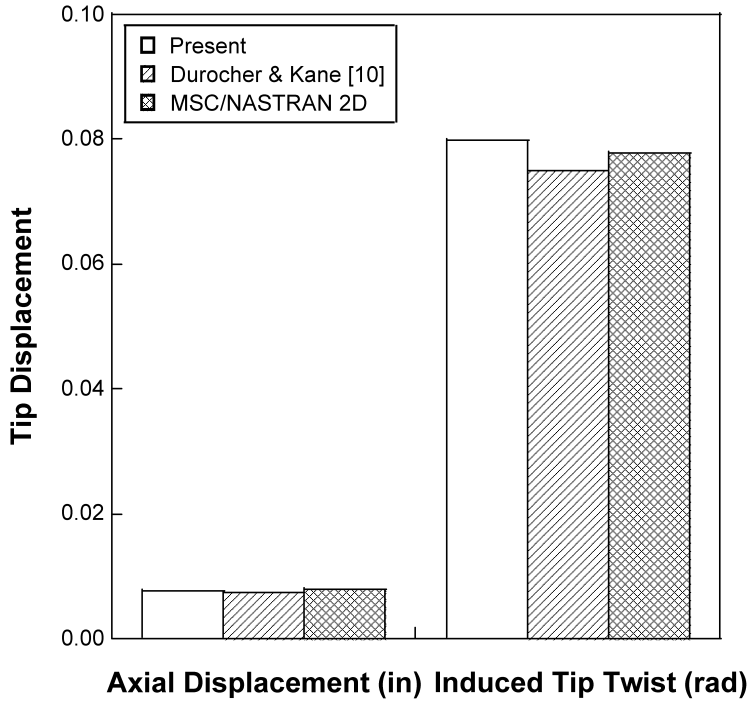


**Figure 4.** Comparison of response for pretwisted rectangular solid beam under tip tension (22 250 N).

the pretwisted beam under the action of tip tensile load amounting 22 250 N. The present results are compared with the analysis results obtained by Durocher and Kane [10] and with two-dimensional shell finite element analysis results using the MSC/NASTRAN. A total of 200 CQUAD4 elements are used for the NASTRAN analysis. As is expected, the pretwisted beam presents a geometrically coupled response between extension and torsion. It is seen that the present theory captures the coupled response satisfactorily. The agreement between the three different results appears acceptable. In general, the present results with the mixed formulation are in a better agreement with the NASTRAN results than those predicted by Durocher and Kane [10]. Figure 5 shows the comparison of both the tip twist and induced tip tension displacements for the cantilevered beam subjected to a tip torque load of 22.6 N m. A good agreement is obtained in comparison with Durocher and Kane and NASTRAN analysis results.

The next example is a rectangular solid section beam with elastic couplings. The schematic of the beam is presented in Fig. 6. The length is 254 mm while the width and height of the beam are 25.4 mm and 2.54 mm, respectively. The beam section is composed of $[\theta_3/-\theta_3]$ to result in an extension–torsion coupling. The positive fiber angles are defined as the right angle from the top surface of the beam (see Fig. 6). The mechanical material properties of a graphite-epoxy lamina used for the beam are summarized in Table 1.

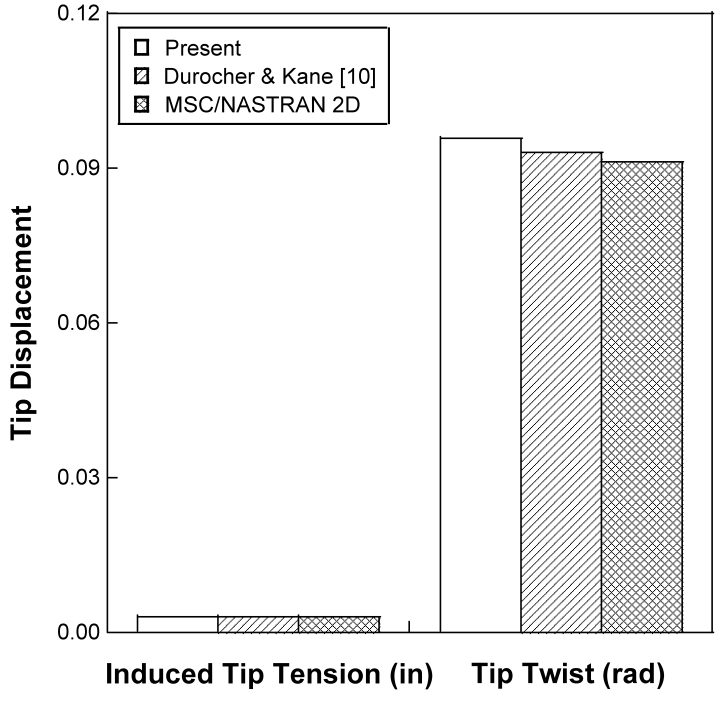


**Figure 5.** Comparison of response for pretwisted rectangular solid beam under tip torque (22.6 N m).

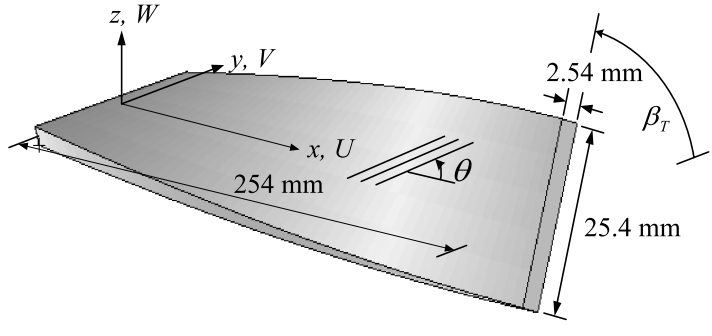


**Figure 6.** Geometry of composite beams with rectangular solid section.

Figure 7 shows the comparison of the direct tip response obtained by the present mixed beam theory and a two-dimensional MSC/NASTRAN analysis for composite beams subjected to a tensile load of 1000 N. A total of 160 CQUAD4 plate/shell elements are used for the NASTRAN calculation. In Fig. 7, the tip axial displacements are presented as a function of pretwist angles while the fiber angles $\theta$ are varied from 0 to 90°. The correlation between the present results and the NASTRAN predictions is seen to be excellent. It is indicated that both the fiber angles and the pretwist angles affect the beam behavior significantly. As the pretwist angle varies from 0 to 90°, a maximum of 60% increase in the tip axial displacement is

**Table 1.**
Mechanical properties of graphite-epoxy lamina

| Properties | Values |
|---|---|
| $E_{11}$ | 141.9 GPa |
| $E_{22}$ | 9.78 GPa |
| $G_{12}$ | 6.13 GPa |
| $\nu_{12}$ | 0.42 |
| Ply thickness | 0.127 mm |

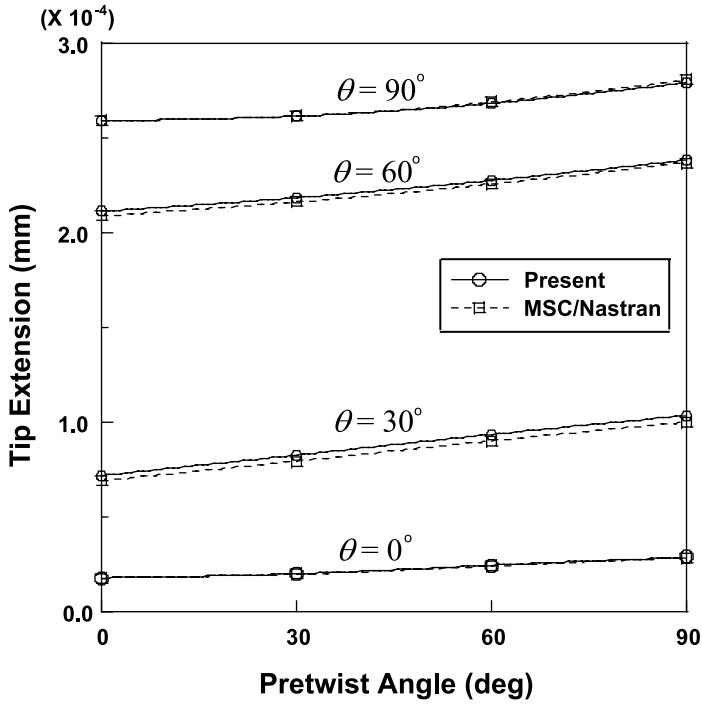


**Figure 7.** Comparison of tip axial displacements with respect to pretwist angles for composite beams under a tensile load (1000 N).

attained at a layup angle of zero degrees. In addition, as much as 1.348% increase of tip tension is obtained at the zero pretwist angle as the fiber angle is changed from 0 to 90°. Figure 8 shows the induced tip twist deformation predicted by the present theory and the NASTRAN analysis for the same beam undergoing tensile load of 1000 N. The correlation between the two results appears fair to good for this case. Results with four different layup cases are presented together to show and quantify the effect of fiber angles. It is observed that the induced response of the pretwisted beam is highly dependent upon the layup angles adopted in the wall of the beam. This implies that the elastic couplings introduced by the non-zero ply an-

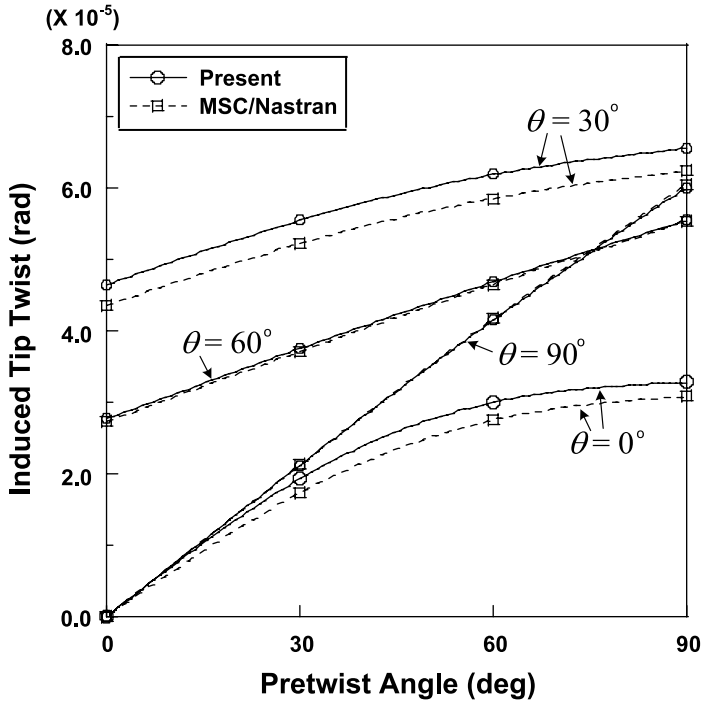


**Figure 8.** Comparison of induced tip twist angles with respect to pretwist angles for composite beams under a tensile load (1000 N).

gles play significant roles for the induced beam behavior. The geometric couplings arising due to the pretwist angles are combined with the effect of elastic couplings to make the analysis more complicated. As can be found in Fig. 8, untwisted beams with non-zero ply angles show a purely elastic behavior. The magnitude of elastic couplings is biggest when the ply angle is set to 30°.

In Fig. 9, the direct tip response of composite beams under a tip torque load of 113 N m is presented as a function of pretwist angles. As in the previous cases, the present results are compared with those by NASTRAN analysis. The correlation is poor for the 0-degree beam while the remaining cases appear acceptable. The reason for a fairly large discrepancy in the zero degree case is unclear at this time but the local distortion effect that might occur in the NASTRAN analysis could be a possible source of the error. It is believed that the discrepancy is not associated with the modeling of pretwist since the error is biggest for beams with no pretwist. For better correlation, a more refined representation of torsion warping in the beam model is necessary to capture the higher order distortion effect associated with the torsion.

Figure 10 shows the induced axial displacements denoted as a function of pretwist angles for rectangular solid section beams subjected to a torque load of 113 N m. Even though the respective magnitudes are different, the induced behavior

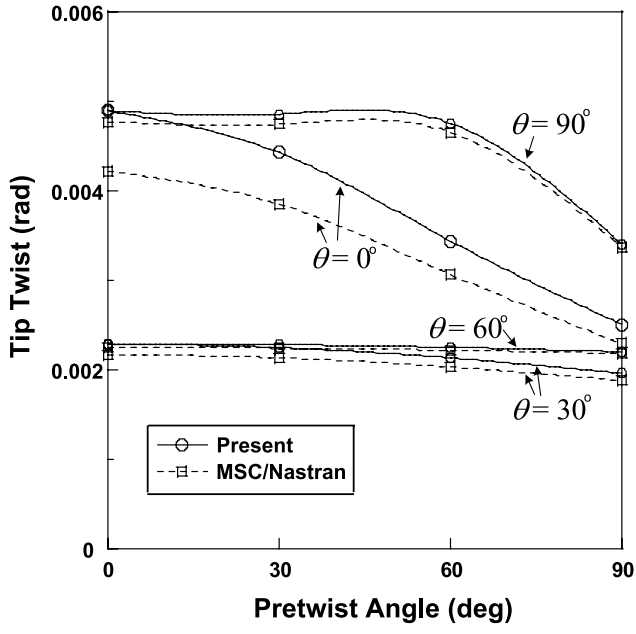


**Figure 9.** Comparison of tip twist angles with respect to pretwist angles for composite beams under a torque load (113 N m).

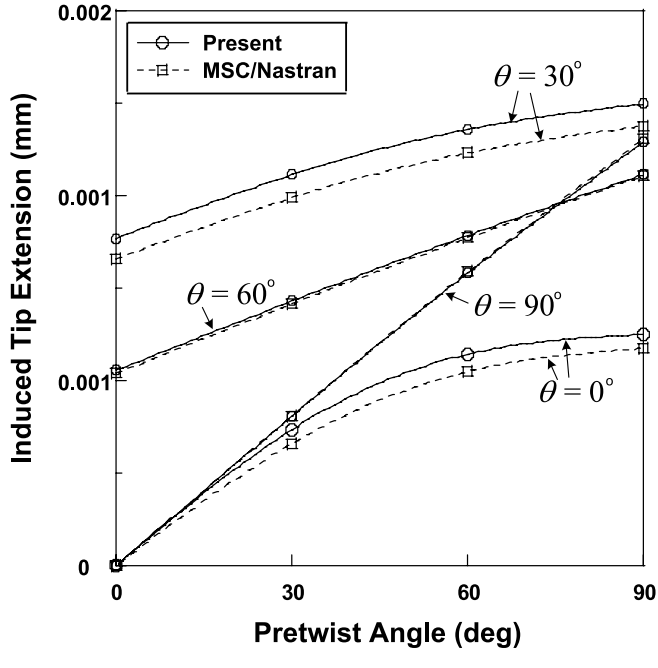


**Figure 10.** Comparison of induced tip tension with respect to pretwist angles for composite beams under a torque load (113 N m).

seems identical as that with Fig. 8. This is because the beam has only tension–torsion couplings due to the geometric and elastic origin that lead to an identical tension–torsion coupled response.

Figures 11–13 present responses of pretwisted beams undergoing tip tension or tip torque load as a function of ply orientation angles. As in the previous cases, the wall of the beam is constructed as: $[\theta_3/-\theta_3]$. Figure 11 shows the direct tip axial response with changing pretwist angles. As the pretwist angle is increased from 0 to 90°, the tip displacements become larger. Thus, a softening behavior is noticed with increasing pretwist angles. In Fig. 12, the direct tip twist response is plotted with respect to ply angle changes. In contrast to the tensile response, the tip twist deformation becomes reduced as the pretwist angles are increased, i.e., a stiffening behavior is obtained with an increase of the pretwist angles. Figure 13 shows the induced response presented as a function of ply angles. It is indicated that, for the untwisted ($\beta_T = 0$) beam, the induced response is purely dominated by the elastic couplings introduced by the non-zero ply angles of the beam. With the introduction of pretwist angles, however, both the elastic and geometric tension–torsion couplings combine to play substantial roles in the beam behavior.

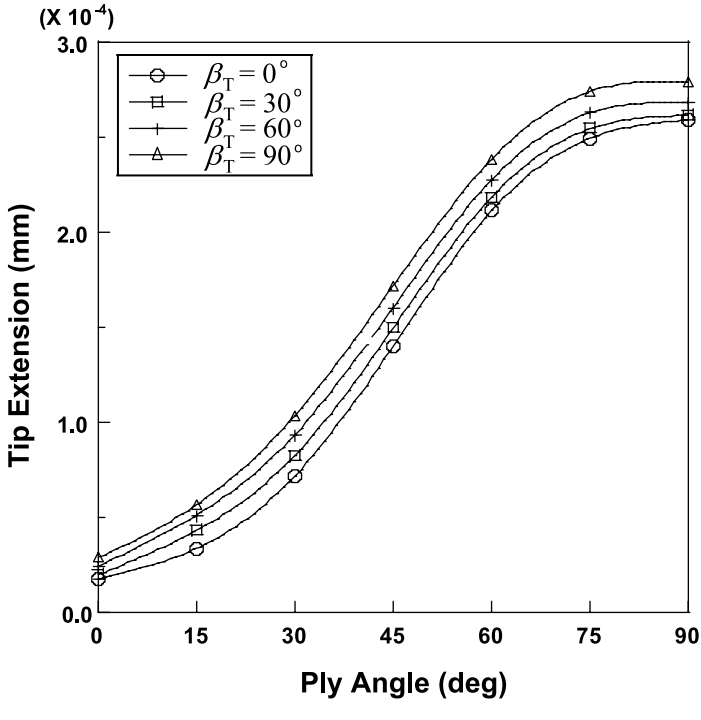


**Figure 11.** Effect of pretwist angles on tip axial displacements of composite beams under a tensile load.

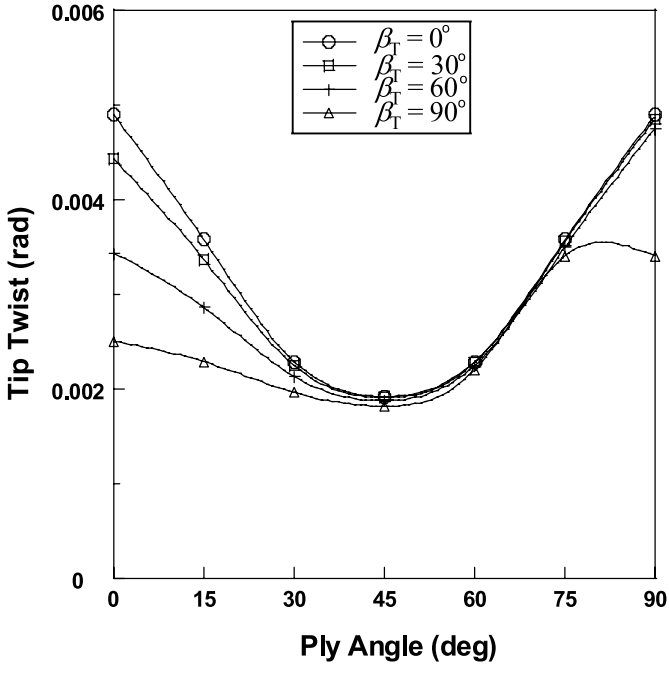


**Figure 12.** Effect of pretwist angles on tip twist angles of composite beams under a torque load.

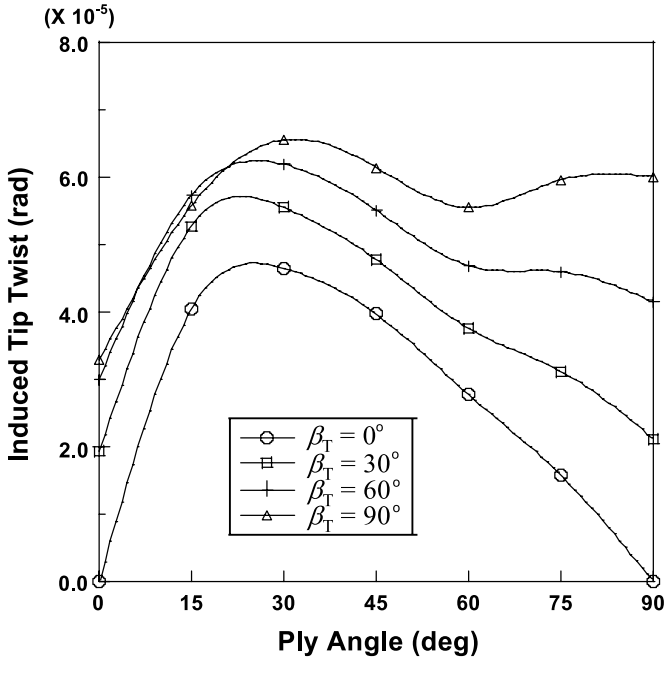


**Figure 13.** Effect of pretwist angles on induced response of composite beams under a tensile load.

## 4. Conclusions

In the present work, a mixed beam formulation for thin-walled composite beams with built-in pretwist has been developed. The beam force–displacement relations were obtained by using the Reissner semi-complementary energy functional. The bending and torsion-related warpings introduced with the pretwist effect were derived in closed form in the beam formulation. The theory was validated with available literature and detailed finite element results using the two-dimensional MSC/NASTRAN analysis. Rectangular solid section beams with and without elastic couplings were considered in the comparison study. Overall, an acceptable correlation of responses with NASTRAN predictions was obtained except a direct torsion case. It was found that the discrepancy was not related with the modeling of pretwisted effect but a more refined representation of warping models associated with torsion appeared necessary toward a better correlation. The effects of pretwist and fiber orientation angles on the static behavior of composite beams were also investigated. It was found that both the fiber angles and pretwist angles affected the beam behavior significantly. More than 1.300% increase of direct tip displacements was attained with changing ply orientation angles while a maximum of 60% increase in the beam response was noticed with respect to the pretwist angle changes.

*Acknowledgements*

This work was supported by the faculty research fund of Konkuk University in 2006.

## References

1. Rosen, Structural and dynamic behavior of pretwisted rods and beams, *Appl. Mech. Rev.* **44**, 483–515 (1991).
2. E. S. Cesnik, D. Hodges and V. G. Sutyrin, Cross-sectional analysis of composite beams including large initial twist and curvature effects, *AIAA J.* **34**, 1913–1920 (1996).
3. A. Bauchau and C. H. Hong, Large displacement analysis of naturally curved and twisted composite beams, *AIAA J.* **25**, 1469–1475 (1987).
4. P. F. Pai and A. H. Nayfeh, A fully nonlinear theory of curved and twisted composite rotor blades accounting for warping and three-dimensional stress effects, *Intl. J. Solids Struct.* **9**, 1309–1340 (1994).
5. W. Yu, *Variational Asymptotic Modeling of Composite Dimensionally Reducible Structures*, PhD Thesis, Georgia Institute of Technology, Atlanta, GA, USA (2002).
6. V. V. Novozhilov, *Thin Shell Theory*, P. Noordhoff, Inc., The Netherlands (1964).
7. S. N. Jung, V. T. Nagaraj and I. Chopra, Refined structural model for thin- and thick-walled composite rotor blades, *AIAA J.* **40**, 105–116 (2002).
8. S. N. Jung, I. J. Park and E. S. Shin, Theory of thin-walled composite beams with single and double-celled sections, *Composites Part B: Engng* **38**, 182–192 (2007).
9. Gjelsvik, *The Theory of Thin Walled Bars*. Wiley, New York, USA (1981).
10. L. L. Durocher and J. Kane, A preliminary design tool for pretwisted, tapered beams for turbine blades, *Trans. ASME, J. Mech. Design* **102**, 742–748 (1980).